JOURNAL OF GEOPHYSICAL RESEARCH, VOL. 104, NO. B11, PAGES 25,611–25,622, NOVEMBER 10, 1999

Widespread extension in the core of the western Alps revealed by earthquake analysis

Christian Sue,[1] François Thouvenot, and Julien Fréchet

Laboratoire de Géophysique Interne et Tectonophysique, Observatoire de Grenoble, Grenoble, France

Pierre Tricart

Laboratoire de Géodynamique des Chaînes Alpines, Grenoble, France

Abstract. The western Alps are an active collision belt whose current stress field is inhomogeneous [*Müller et al.,* 1992]. We report new seismological data which significantly improve our knowledge of this stress field. About 1600 earthquakes which occurred in the western Alps during the last 10 years were precisely located, and 79 new focal solutions were computed. The analysis of this database shows that widespread extension affects all the internal zones of the belt. To better constrain the associated stress regime, six stress tensors were computed using the *Gephart and Forsyth* [1984] method. They show that the current tectonics of the western Alps are contrasted with close variation in the stress regime (transpression to the front of the belt contrasting with extension in the core of the belt). The extensional direction is radial to the arcuate geometry of the belt and bounded outboard by the former thrust of the internal zones onto the external zone, suggesting extensional reactivation of this inherited crustal discontinuity. Such widespread extension within the inner part of an actually ongoing collision belt cannot be explained by simple collision-related tectonics. We propose that intrabelt buoyancy forces, such as those produced by a slab retreat or slab break-off, interfere with the boundary forces driven by the ongoing Europe-Africa convergence.

1. Introduction

The western Alps result from the Europe-Africa collision, which leads to the indentation of Europe by the Adriatic promontory (Adria) [*Tapponnier,* 1977], with a probable counterclockwise rotation of the indenter [*Anderson and Jackson,* 1987; *Ménard,* 1988; *Vialon et al.,* 1989]. One of the major structures related to this indentation is a crustal-scale thrust of Oligocene age (~ 30 Ma) [*Tricart,* 1984], which brings the internal (Penninic) metamorphic zones onto the external zone (Crustal Penninic Front, CPF), underlining the arcuate geometry of the belt (Figure 1). Present-day convergence velocity is less than 1 cm.yr^{-1} [*DeMets et al.,* 1990], and seismicity is currently moderate and inhomogeneous in the western Alps. The first seismotectonic studies in the Alps [e.g., *Fréchet,* 1978; *Fréchet and Pavoni,* 1979; *Pavoni,* 1980; *Pavoni and Roth,* 1990] linked horizontal P axes of earthquake focal mechanisms to the directions of crustal shortening as inferred from structural analysis. Thus, it was proposed that the dynamics of the current belt remained unchanged since the Tertiary. Nevertheless, several seismotectonic investigations found normal-faulting focal solutions in different regions of the western Alps: in the southwestern Alps [*Fréchet,* 1978; *Fréchet and Pavoni,* 1979], in the Italian Alps [*Eva et al.,* 1997], and in the Swiss Alps [*Roth et al.,* 1992; *Maurer et al.,* 1997]. These areas affected by extension were thought to be limited. However, these deviations from a purely compressive stress field showed that the tectonics of the western Alps are much more complex than expected. *Eva et al.* [1998] recently published a tectonic sketch map of the northern part of the western Alps showing extension in a rather large part of the Penninic nappes (internal zones).In this paper we provide new seismotectonic data from the western Alpine arc as a whole, from the Mont Blanc massif to the Argentera massif, along 250 km (Figure 1). We show that the main part of the deformation in the internal zones is actually extensional. This large-scale extension calls for a new geodynamic model for the western Alps

2. Data Analysis

Earthquakes are the most obvious expression of ongoing tectonic activity in the western Alps. They are monitored by the 44-station Sismalp seismic network [*Thouvenot et al.,* 1990] (Grenoble Observatory, France) and the 10-station IGG network (Geophysical Institute of Genova, Italy). Figure 1 shows the seismic stations available in the inner zones against a tectonic sketch map of the main Alpine structures. Most stations are equipped with 1-Hz vertical seismometers; three-component seismometers are operated in five stations.

Alpine seismicity is relatively moderate in comparison to other active belts (Figure 2a), with local Richter magnitudes (M_L) typically ranging from 1 to 4. Systematic study of Alpine seismicity over the last decade shows that most earthquakes occur along two seismic arcs (Figure 2a). The Briançonnais seismic arc (beneath the Briançonnais Zone, east of the CPF) and the Piemont seismic arc (between the Dora-Maira and Argentera

[1]Also at Laboratoire de Géodynamique des Chaînes Alpines, Grenoble, France; now at Institut de Géologie, Université de Neuchâtel, Neuchâtel, Switzerland.

Paper number 1999JB900249.
0148-0227/99/1999JB900249$09.00

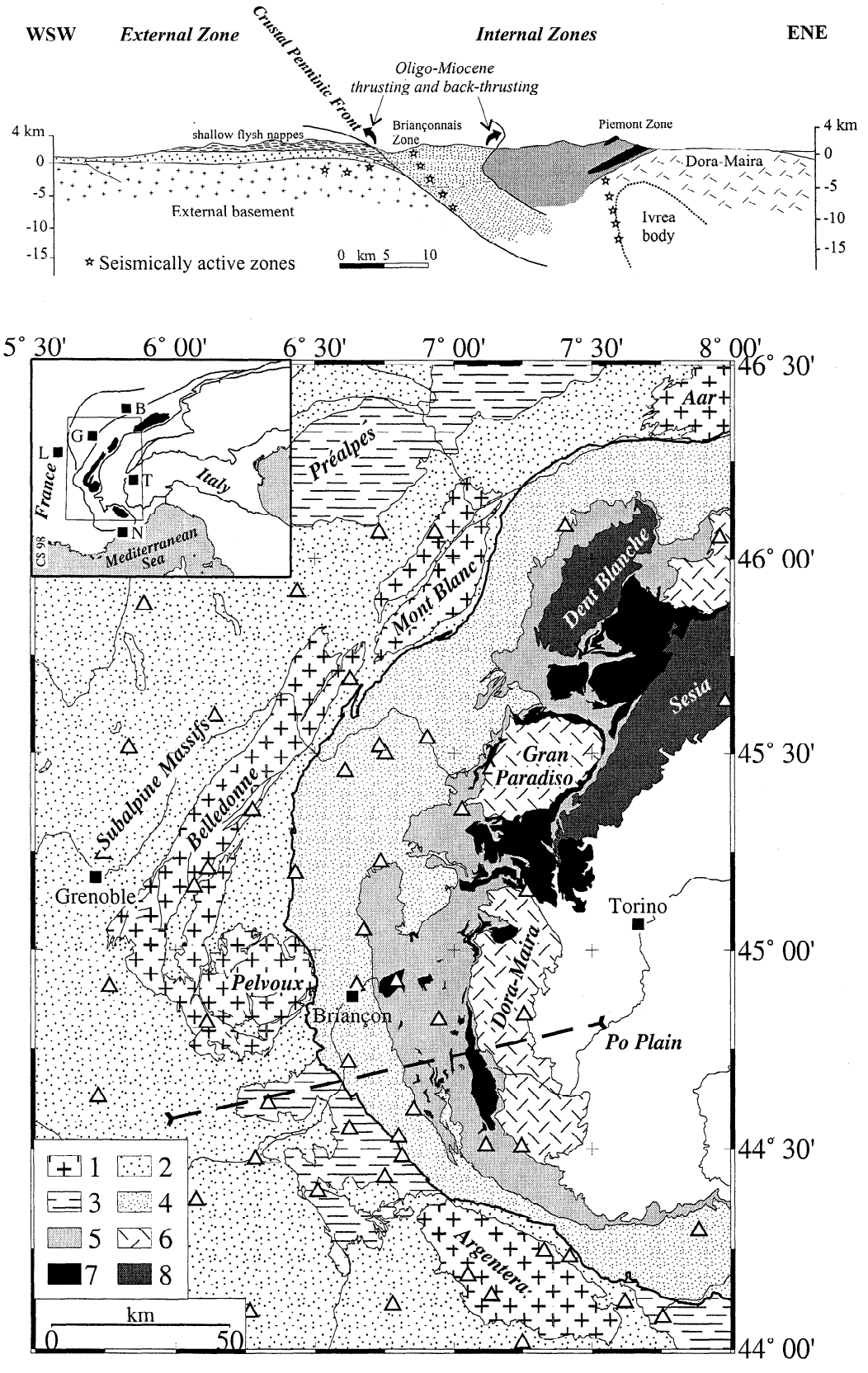

Figure 1. Structural map of the western Alps. Triangles show seismological stations used in this study (Sismalp and IGG networks). The ENE-WSW interpretative cross section, after *Tricart* [1984], shows the main structures and thrust zones to the south of the Pelvoux massif. Stars indicate present-day active zones in the upper crust. The position of the cross section is marked on the map (thick lines). Symbol legend is 1, external crystalline massifs (ECM); 2, Meso-Cenozoic sedimentary cover of ECM; 3, internal nappes thrust onto the external zone (in particular, pellicular flysch nappes); 4, Briançonnais Zone; 5, Piemont Zone; 6, internal crystalline massifs; 7, main ophiolites; 8, Austro-Alpine units; the Crustal Penninic Front (CPF) is represented by the bold line. Towns are B, Bern; G, Genève; L, Lyon; N, Nice; T, Torino.

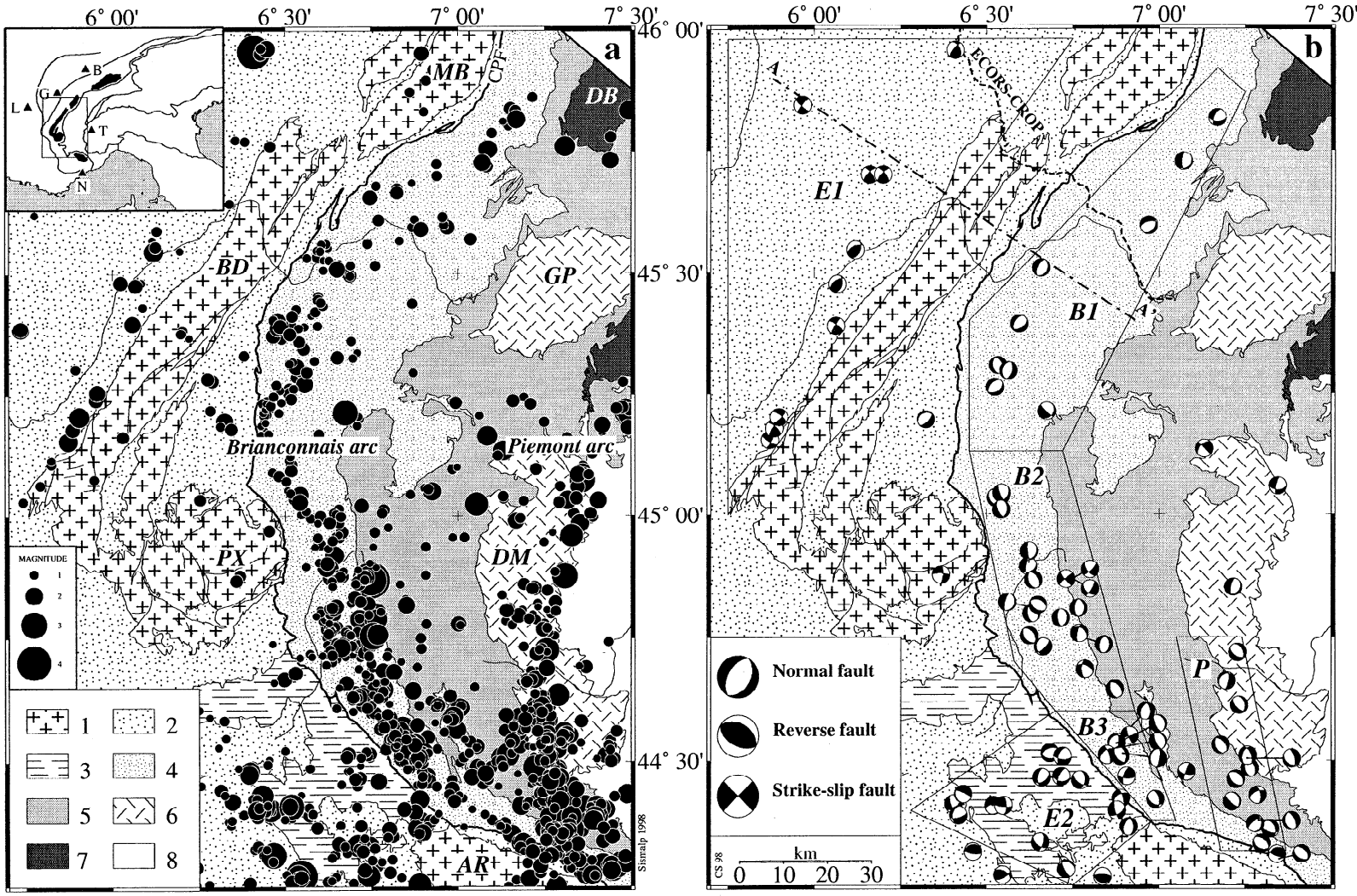

Figure 2. Seismicity and seismotectonic maps of the western Alps with main structural units. Same symbols as Figure 1. (a) Earthquakes recorded by the Sismalp and IGG seismic networks between 1989 and 1997. Only events with M_L>1, root-mean-square residual smaller than 1 s and azimuthal gap smaller than 180° are plotted. The Briançonnais seismic arc is located beneath the Briançonnais Zone (tightly set stippling), just east of the CPF (bold line); the Piemont seismic arc is located between the Dora-Maira (DM) and Argentera (AR) massifs. (b) Seismotectonic map showing reliable focal mechanisms computed with the same database. Six seismic domains have been defined using structural considerations: *E1* and *E2* in the external zone; *B1, B2,* and *B3* along the Briançonnais seismic arc; and *P* along the Piemont seismic arc. All domains except *E1* undergo extension, whereas *E1* undergoes transpression. Dashed curve corresponds to ECORS-CROP seismic profile, and dashed line AA' to the cross section of Figure 4.

massifs) [*Rothé*, 1941] concentrate most of this upper crust seismicity (0-20 km depth). Earthquakes recorded by the Sismalp and IGG seismic networks between 1989 and 1997 are plotted in Figure 2a; epicenters were computed using a modified version of the Hypo71 software [*Lee and Lahr*, 1975] to take into account secondary arrivals and station altitudes. *S* wave readings were included when available. Only events with $M_L>1$, root-mean-square (rms) residual smaller than 1 s and azimuthal gap smaller than 180° are plotted.

For routine locations the Grenoble Observatory has commonly used a simple three-layer velocity model since the Sismalp network was installed 10 years ago. This model was derived from previous deep-seismic-sounding experiments. In this study we used the 12-layer velocity model computed by *Sellami et al.* [1995] for the western Alps. This one-dimensional (1-D) velocity model uses the three-layer model as a starting point in a trial-and-error procedure which minimizes the rms residual for a set of well-recorded and well-located earthquakes. It improves the routine locations obtained when using the three-layer model and provides a high-quality data set. Earthquakes selected for this study (Table 1) have a small rms (0.38 s on the average) and small horizontal and vertical uncertainties (0.6 km and 1.1 km respectively on the average). These uncertainties mainly reflect, from a statistical viewpoint, the consistency of arrival times, and they do not take into account variations in the velocity model. Real horizontal and vertical uncertainties may thus be larger than those listed in Table 1.

To check this, *Sue* [1998] compared locations computed when using successively three velocity models: the three-layer model, the 12-layer model, and a 3-D model derived by *Paul et al.* [1998] for the region between the Pelvoux and Argentera massifs. For the Briançonnais seismic arc, *Sue* [1998] concluded that neither epicenters nor focal mechanisms depend significantly on the input model (epicenters fall within about 1 km in distance), the critical parameter being the focal depth which varies by up to 2 km on average. For the Piemont seismic arc, *Paul et al.* [1998] showed that earthquake parameters, including the focal depth, remain quite stable when using either the 12-layer model or the 3-D model. Thus it seems finally sound to rely on locations and focal depths listed in Table 1 for studying now more thoroughly both seismic arcs. Despite the low magnitude of most events, we will demonstrate that our data set is very homogeneous in terms of stress analysis. Moreover, *Amelung and King* [1997] have shown that the tectonic interpretations drawn from small earthquakes are reliable and very close to the interpretations drawn from large ones. We can thus rely on this microseismicity to draw robust tectonic interpretations, although the associated deformation remains low.

Earthquakes along the 250-km-long Briançonnais arc mainly have focal depths between 0 and 15 km and coincide fairly well with the arcuate geometry of the CPF, suggesting the current reactivation of this Oligocene thrust, at least from the Mont-Blanc to the Argentera massifs. In contrast, the Piemont seismic arc, in an innermost position in the western Alps, has deeper hypocenters (in the 10-20 km range), is straighter, shorter (100 km), and crosscuts the trend of surface structures. It involves deep structures such as the mantle slice known as the Ivrea body, identified and modeled using gravity [*Ménard and Thouvenot*, 1984; *Rey et al.*, 1990], deep-seismic-sounding data [*ECORS-CROP Deep Seismic Sounding Group*, 1989], and tomography [*Solarino et al.*, 1997; *Paul et al.*, 1998].

From a seismotectonic viewpoint (Figure 2b), six tectonic domains can be defined using structural considerations. *E1* and *E2* are located in the external zone; *E1* west of the Belledonne and Mont-Blanc massifs, and *E2* between the Pelvoux and Argentera massifs, i.e., beneath pellicular flysch nappes. In the internal zones, domains *B1*, *B2*, and *B3* are situated in the Briançonnais Zone, while *P* straddles the Dora-Maira massif and the Piemont Schistes Lustrés Zone. Focal mechanisms previously computed for the *E1* domain [*Thouvenot*, 1996] (Table 2) indicate a transpressive tectonic regime, in good agreement with known features of the kinematics related to Tertiary Alpine collision [*Coward et al.*, 1989; *Ménard*, 1988] and with large-scale stress maps [*Grünthal and Stromeyer*, 1992; *Müller et al.*, 1992]. The strike-slip focal mechanisms in this domain result from dextral transcurrent movements [*Ménard*, 1988], longitudinal to the belt, and probably linked to the counterclockwise rotation of the Adriatic indenter with regard to stable Europe. The main result of our seismotectonic analysis is that the large majority of the focal mechanisms we computed for the internal zones indicate normal faulting.

Figure 2b presents a seismotectonic map showing the 79 (numbers 1-79) reliable focal mechanisms computed with our database and using the FPFIT software [*Reasenberg and Oppenheimer*, 1985]. The corresponding stereonets are plotted on Figure 3, and Table 1 lists the corresponding parameters. Figure 2b also shows the 10 (numbers 80-89) focal mechanisms previously computed for the *E1* domain by *Thouvenot* [1996]. Table 2 lists the corresponding parameters. The inset map in Figure 3 gives the position of the 89 focal mechanisms. For each of the 79 new focal mechanisms computed in this study, we required more than 10 polarity readings with a fairly homogeneous azimuthal distribution. We also discarded non-unique and badly constrained solutions.

The focal solutions of the B2 domain generally have E-W trending *T*-axes. This is compatible with the result of C. Sue et al. (Active deformation on the inner western Alps inferred from comparison between 1972-classical and 1996-GPS geodetic surveys, submitted to Tectonophysics, 1999), who inferred active deformation in the same area from geodetic measurements, indicating E-W orientation of reliable extensional strain axes.

The cross section drawn across the *E1* and *B1* domains (Figure 4) clearly indicates that *B1* earthquakes are located in the hangingwall of the CPF (equivalent in this part of the Alps to the Penninic Frontal Thrust imaged by the ECORS-CROP seismic profile [*Nicolas et al.*, 1990]). The difference between the CPF and the classical Penninic Frontal Thrust concerns only the region between the Pelvoux and Argentera massifs. The Penninic Frontal Thrust bounds to the west sedimentary cover pellicular nappes (flysch nappes, see symbol caption 3 on Figure 1). On the contrary, the Crustal Penninic Front (CPF, bold line on Figure 1) better underlines the arcuate geometry of the belt and bounds the Briançonnais Zone to the west (symbol caption 2 on Figure 1). The CPF corresponds to the main crustal discontinuity between internal and external zones in the western Alps. In map view (Figure 2b) as well as on the cross section (Figure 4), most nodal planes of the *B1*, *B2*, and *B3* domains strike parallel to the local trend of the Alpine arc and to the CPF. This suggests that extensional reactivation of the CPF controls the seismic activity in the Briançonnais arc. *Sue and Tricart* [1999] also established a Late Alpine extension close to the CPF, and a possible tectonic inversion of the CPF, from structural analysis of brittle deformation to the SE of the Pelvoux massif. West of the CPF, *E1* earthquakes are located in the crystalline basement beneath

Table 1. Focal Solution parameters for *E2*, *B1*, *B2*, *B3* and *P* Domains

N	D	Date	h	mn	sec	Lat	Lon	Depth	Mag	Gap	rms	erh	erz	phi1	dip1	rk1	phi2	dip2	rk2	phiP	dipP	phiT	dipT
1	P	891030	11	24	6	44-36.7	7-14.0	7.6	3.0	53	0.5	0.6	0.8	225	60	-110	81	36	-59	4	68	239	13
2	P	891202	8	56	31	44-43.1	7-13.7	13.6	1.8	98	0.2	0.7	1.6	210	55	-110	62	40	-64	339	72	224	8
3	B2	891213	8	8	14	44-47.3	6-42.9	9.8	2.3	56	0.2	0.5	0.7	95	30	-80	264	61	-96	69	74	268	15
4		900120	19	25	19	45-08.1	7-07.8	1.6	2.5	41	0.8	0.9	1.8	45	90	-140	315	50	0	188	27	82	27
5	E2	910207	0	46	54	44-25.5	6-53.4	9.7	2.3	29	0.5	0.6	0.8	75	70	-140	329	53	-25	208	42	108	11
6	B2	910211	15	43	43	44-52.1	6-45.0	7.4	4.5	44	0.6	0.7	0.9	135	65	-10	229	81	-165	5	14	270	11
7	B2	910213	12	54	42	44-52.1	6-45.0	6.4	3.8	44	0.4	0.6	1.1	225	45	-160	121	76	-47	341	42	90	19
8	B2	910213	15	49	39	44-52.1	6-45.0	6.4	3.9	44	0.6	0.7	1.1	135	75	-30	234	61	-163	1	32	97	9
9	E2	910423	5	52	38	44-28.1	6-43.0	9.8	1.7	42	0.4	0.5	0.6	185	45	-30	297	69	-131	73	49	326	14
10		910729	8	46	17	44-51.1	7-12.9	12.0	1.6	73	0.4	0.8	1.5	135	25	-60	283	69	-103	81	64	293	22
11	B3	910812	22	56	9	44-48.2	6-46.0	2.7	2.2	39	0.6	0.7	1.4	90	35	-90	270	55	-90	90	80	270	10
12	B3	911127	12	18	26	44-31.4	6-51.7	9.1	1.6	46	0.4	0.6	0.9	85	50	-110	295	44	-68	200	74	99	3
13	E2	920102	2	12	26	44-24.8	6-26.1	8.3	2.3	110	0.3	0.6	0.8	140	55	-30	248	66	-141	18	44	282	7
14	E2	920411	6	56	52	44-27.9	6-42.3	9.4	1.6	49	0.3	0.4	0.6	150	50	-50	278	54	-127	37	60	303	2
15		921109	13	11	39	44-18.8	7-20.7	15.1	1.8	79	0.4	0.7	1.2	200	70	110	333	28	47	185	22	49	60
16	P	921111	0	59	53	44-29.1	7-15.8	9.5	2.1	63	0.6	1.0	1.5	260	45	-80	66	46	-100	166	83	73	0
17	P	930215	12	15	3	44-20.1	7-18.0	12.3	1.9	56	0.6	0.9	1.3	205	40	-100	38	51	-82	262	82	32	5
18	P	930315	23	43	29	44-21.8	7-19.4	13.1	3.4	58	0.6	0.6	0.7	200	55	-120	65	45	-54	323	65	221	6
19	B3	930322	4	27	3	44-28.1	6-54.3	8.5	1.6	49	0.3	0.4	0.6	185	65	150	289	63	28	147	1	56	38
20	P	930407	16	36	3	44-25.1	7-12.8	9.3	1.5	78	0.4	0.7	1.3	220	75	-100	74	18	-57	26	59	228	29
21	P	930410	17	54	25	44-25.9	7-17.2	15.1	1.8	85	0.4	0.6	1.6	335	60	-30	81	64	-146	210	41	117	3
22		930505	4	34	1	44-16.1	6-50.2	10.4	1.2	51	0.3	0.5	1.9	205	25	110	3	67	81	10	21	166	67
23	B3	930615	15	0	22	44-31.3	6-51.4	7.4	1.6	46	0.4	0.6	1.4	245	70	-90	65	20	-90	65	65	245	25
24	B2	930710	20	3	59	44-53.6	6-37.2	2.8	2.2	31	0.4	0.5	1.1	155	35	-40	280	68	-118	61	57	300	19
25	B1	930721	1	59	16	45-30.5	6-39.5	3.8	2.4	60	1.0	1.1	1.4	115	30	-90	295	60	-90	115	75	295	15
26	E2	931021	15	30	17	44-24.0	6-52.7	10.6	1.9	33	0.2	0.3	0.7	150	55	-20	252	74	-143	26	37	287	12
27	B2	931030	5	45	12	44-47.8	6-37.8	5.6	1.2	77	0.3	0.5	1.5	260	55	-70	48	40	-116	131	72	246	8
28	B2	931110	19	13	17	44-45.1	6-37.4	8.5	1.4	44	0.4	0.6	1.0	230	45	-90	50	45	-90	301	90	50	0
29	B1	931122	3	28	54	45-35.7	6-58.2	6.6	1.8	129	0.5	0.7	1.1	130	35	-120	345	60	-71	205	69	331	13
30	B2	931214	3	7	7	45-02.3	6-32.5	7.1	1.9	32	0.4	0.5	1.0	100	25	-70	258	67	-99	61	67	265	21
31		940209	8	33	23	45-03.5	7-20.7	15.7	1.8	83	0.8	1.5	3.8	180	50	-20	283	75	-138	60	40	316	16
32	E2	940211	11	35	23	44-22.1	6-54.7	6.8	1.5	37	0.3	0.4	1.4	85	45	-110	292	48	-71	182	76	279	2
33	P	940305	8	12	2	44-27.8	7-13.4	14.4	1.4	81	0.3	0.5	1.0	220	50	-90	40	40	-90	40	85	220	5
34	E2	940415	2	58	13	44-17.0	6-43.9	6.3	1.8	42	0.4	0.5	1.1	240	75	-70	5	25	-142	85	56	224	27
35	B2	940618	4	59	58	44-51.9	6-38.2	9.2	1.2	42	0.2	0.4	0.6	250	45	-80	56	46	-100	156	83	63	0
36	B3	940622	23	8	36	44-33.1	6-54.8	11.2	1.8	49	0.4	0.5	0.6	160	85	-10	251	80	-175	25	11	116	3
37	E2	940627	17	48	48	44-26.0	6-26.0	7.2	2.7	19	0.7	0.6	0.9	255	15	-40	24	80	-102	190	53	34	34
38		940801	21	39	26	45-11.8	6-19.4	1.1	2.1	38	0.5	0.6	1.8	135	65	-100	338	27	-70	295	68	142	19
39	B2	940916	17	58	11	44-38.6	6-52.3	6.1	2.1	67	0.2	0.4	0.8	250	50	-70	41	44	-112	135	74	236	3
40	B2	940917	11	46	60	45-02.1	6-31.6	8.7	1.5	35	0.2	0.4	0.9	225	35	-100	57	56	-83	262	78	52	10
41	B3	940924	4	18	18	44-32.2	6-52.6	3.6	2.5	66	0.4	0.5	1.3	95	70	-110	322	28	-47	246	60	110	22
42		941113	0	36	5	44-19.1	6-27.6	7.1	1.4	69	0.3	0.6	1.0	190	70	100	343	22	64	182	24	26	64
43	E2	941128	8	28	14	44-20.2	6-39.4	9.2	1.8	41	0.3	0.5	0.8	105	60	-40	218	56	-143	340	48	72	2
44	P	941207	21	45	37	44-31.8	7-10.7	12.9	1.8	78	0.2	0.5	0.9	250	40	-70	45	53	-106	173	76	56	7
45	B1	950421	18	19	31	45-43.6	7-04.2	13.7	2.1	176	0.4	0.9	1.4	135	20	-50	273	75	-103	75	58	284	29
46	P	950424	0	39	40	44-39.6	7-11.7	11.4	1.8	106	0.2	0.4	1.3	100	70	-110	327	28	-47	251	60	115	22
47	B2	950911	22	55	53	44-41.1	6-47.1	5.0	1.9	67	0.3	0.5	0.9	270	60	-40	23	56	-143	145	48	237	2
48	P	951007	19	15	1	44-22.4	7-16.8	13.0	2.1	81	0.3	0.6	1.0	100	30	-130	324	68	-70	176	62	309	20
49	B3	951008	6	7	47	44-30.8	6-53.7	4.8	2.1	67	0.3	0.5	1.0	100	75	-90	280	15	-90	280	60	100	30
50	B3	951013	22	7	42	44-30.7	6-50.9	6.1	2.9	64	0.3	0.4	0.8	70	70	-140	324	53	-25	203	42	103	11
51	B3	951018	2	13	9	44-30.5	6-53.3	4.3	2.1	66	0.3	0.4	0.8	225	55	-110	77	40	-64	354	72	239	8
52		951018	12	52	59	44-18.1	7-21.0	15.8	1.8	79	0.2	0.8	0.8	210	45	-100	44	46	-80	304	83	37	0
53	E2	951117	0	48	44	44-30.9	6-41.0	8.3	1.8	45	0.3	0.4	0.6	185	40	-70	340	53	-106	108	76	351	7
54	B2	951122	11	12	53	45-02.6	6-32.6	8.4	2.1	32	0.3	0.5	1.1	130	30	-30	247	76	-117	36	52	267	26
55	P	951124	5	50	17	44-22.8	7-17.4	13.3	1.6	82	0.2	0.4	0.8	255	30	-80	64	61	-96	229	74	68	15
56	E2	951229	2	20	53	44-30.5	6-43.2	7.9	1.2	44	0.2	0.4	0.6	185	65	-40	295	54	-149	55	45	152	6
57	E2	960122	16	41	45	44-27.7	6-46.3	5.4	2.0	55	0.3	0.5	0.8	95	45	-40	216	63	-127	347	55	242	10
58	P	960126	1	0	50	44-30.6	7-15.5	12.9	1.7	87	0.2	0.5	1.1	65	60	-120	294	41	-49	196	62	86	10
59	P	960126	2	19	46	44-30.3	7-15.4	13.8	2.0	87	0.2	0.5	1.0	210	35	-130	76	64	-66	295	63	58	16
60	B2	960218	4	16	33	44-45.2	6-45.3	9.6	3.3	26	0.3	0.4	0.7	90	40	-100	283	51	-82	147	82	277	5
61	B1	960331	5	43	8	45-23.6	6-35.7	8.1	1.2	48	0.3	0.4	1.6	150	50	-70	301	44	-112	35	74	136	3
62	B3	960610	9	2	56	44-32.0	6-52.6	5.4	1.8	47	0.3	0.5	1.0	245	65	-90	65	25	-90	65	70	245	20
63	E2	960809	17	31	16	44-23.4	6-25.1	7.5	1.7	87	0.4	0.7	1.2	165	70	-60	286	36	-144	23	55	143	19
64		960926	11	5	40	44-52.6	6-22.1	6.7	1.5	63	0.4	0.6	2.0	95	70	-170	2	81	-20	227	21	320	7
65	B1	961105	3	32	21	45-15.7	6-31.5	8.0	1.2	49	0.3	0.5	1.2	150	45	-80	316	46	-100	56	83	323	0
66	B1	970219	5	12	54	45-17.8	6-33.8	6.9	1.5	49	0.2	0.4	1.3	105	55	-90	285	35	-90	285	80	105	10
67	B2	970221	19	51	33	44-48.5	6-38.4	8.1	1.8	43	0.3	0.5	1.0	115	20	-80	284	70	-94	98	65	287	25
68	B2	970221	20	1	45	44-48.9	6-38.9	9.9	1.9	36	0.5	0.7	1.0	215	50	-80	20	41	-102	88	81	208	5
69	B3	970301	11	23	20	44-25.3	6-59.4	10.2	1.7	46	0.3	0.6	1.6	205	45	-130	75	57	-57	309	62	52	7
70		970514	17	23	1	44-28.6	7-04.8	9.1	2.0	58	0.2	0.4	0.5	290	85	30	197	60	174	330	17	68	24
71	B1	970515	0	24	4	45-12.8	6-40.5	9.4	3.1	54	0.4	0.7	1.3	125	30	-10	224	85	-120	15	42	248	33
72	B1	970714	2	57	56	45-49.1	7-10.1	14.1	2.2	176	0.6	1.8	1.8	180	55	-40	296	58	-138	60	51	327	2
73	B1	970719	1	25	42	45-17.0	6-32.6	9.8	2.0	38	0.4	0.6	1.2	100	35	-60	245	60	-109	25	69	259	13
74	B2	970803	10	26	25	44-54.2	6-37.3	7.5	1.8	28	0.3	0.5	0.9	135	20	-40	263	77	-106	64	55	276	31
75	B2	970830	6	56	36	44-43.8	6-39.8	8.8	2.2	32	0.4	0.6	1.1	135	70	-70	268	28	-133	344	60	120	22
76	B2	970913	17	59	39	44-45.4	6-46.1	8.8	2.6	37	0.3	0.5	1.2	35	40	-150	281	71	-54	142	50	255	18
77	E2	971022	4	51	9	44-24.6	6-31.3	9.1	2.1	47	0.4	0.6	0.9	110	20	-140	342	77	-74	181	55	329	31
78		971031	4	23	43	44-16.3	6-32.8	5.4	4.0	84	0.4	0.8	1.2	150	60	50	29	48	138	177	7	277	55
79	E2	971106	12	39	48	44-24.6	6-31.1	8.6	3.1	47	0.4	0.6	0.8	185	75	30	87	61	163	223	9	319	32

Dates of events are shown as yymmdd: year, month, day; h is hour; mn is minute; sec is seconds. Location of events are Lat, north latitude; Lon, east longitude; depth (km); mag, local magnitude; gap, azimuthal gap (deg); rms, root-mean-square residual (s); erh, horizontal uncertainty (km); erz, vertical uncertainty (km). Other heads are phi1 (respectively phi2, phiP, phiT) and dip1 (respectively dip2, dipP, dipT): azimuth and dip of the first plane (respectively second plane, *P* axis, *T* axis); rk1 (respectively rk2): rake of the first plane (respectively second plane).

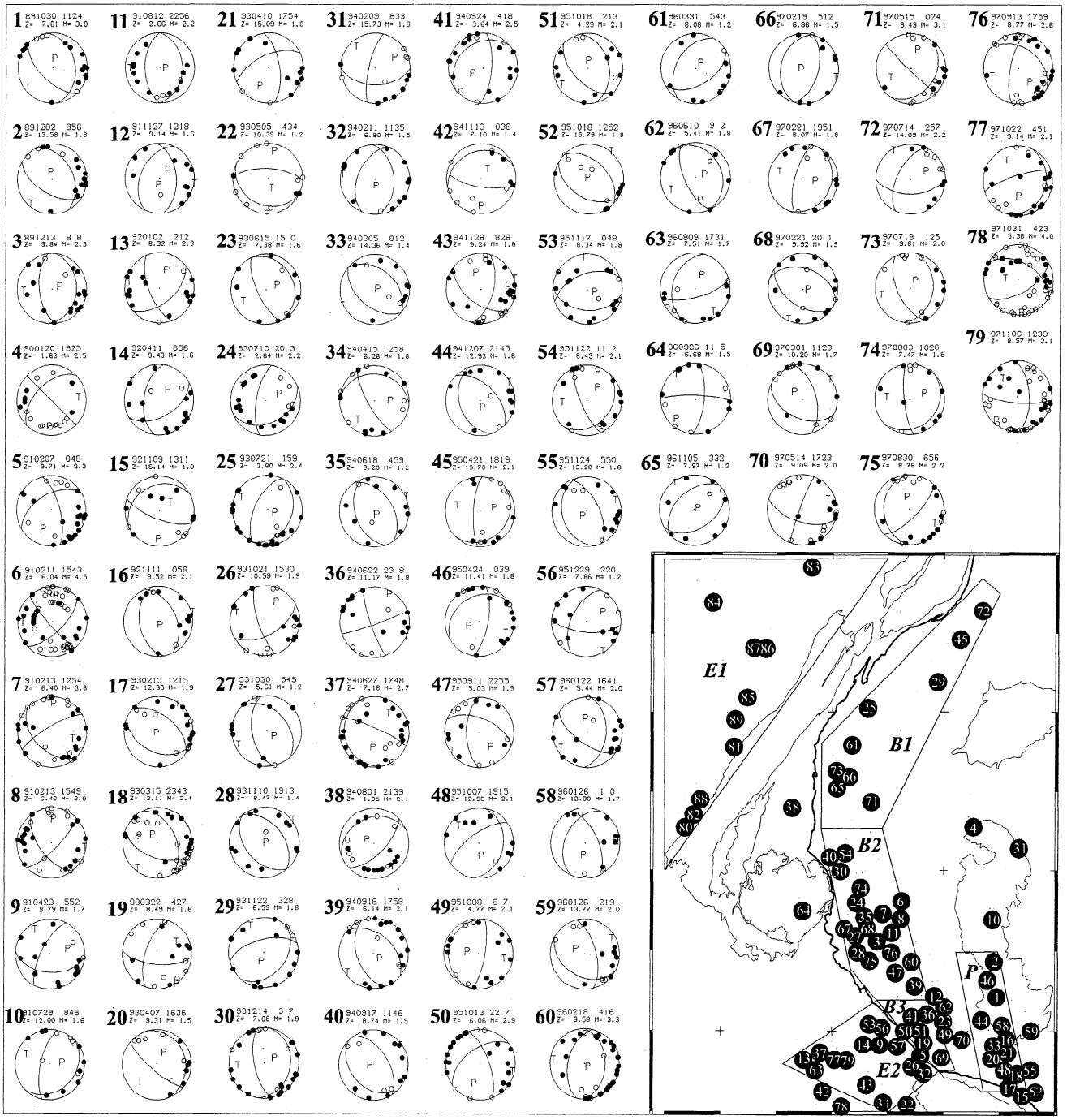

Figure 3. Fault-plane solutions computed for this study. Date of event (yymmdd: year, month, day) refers to Table 1 where focal-solution parameters are listed.

the Mesozoic sedimentary cover, and they imply basement-involved strike-slip and reverse faulting [*Thouvenot*, 1996].

3. Stress-Tensor Inversions

Stress-tensor inversions were performed for each of the six seismotectonic domains, using the method developed by *Gephart and Forsyth* [1984] and *Gephart* [1990]. Results are listed in Table 3, and stress tensors for each of the six seismotectonic domains are plotted on Figure 5. Table 1 indicates which focal mechanisms have been used for these inversions. No selection was applied. Eleven earthquakes were not used for inversion because their epicenters fell outside of the six seismotectonic domains. Misfits computed for the six domains separately are very small (2°-5°), substantiating the a priori regrouping of earthquakes in a given domain. Moreover, if we group several domains such as the internal ones (*B1, B2, B3,* and *P*) or the southern ones (*E2, B3,* and *P*), we obtain larger misfits (around 8°, see Table 3). Thus we point out small but significant changes in the stress field, which appears inhomogeneous in the area

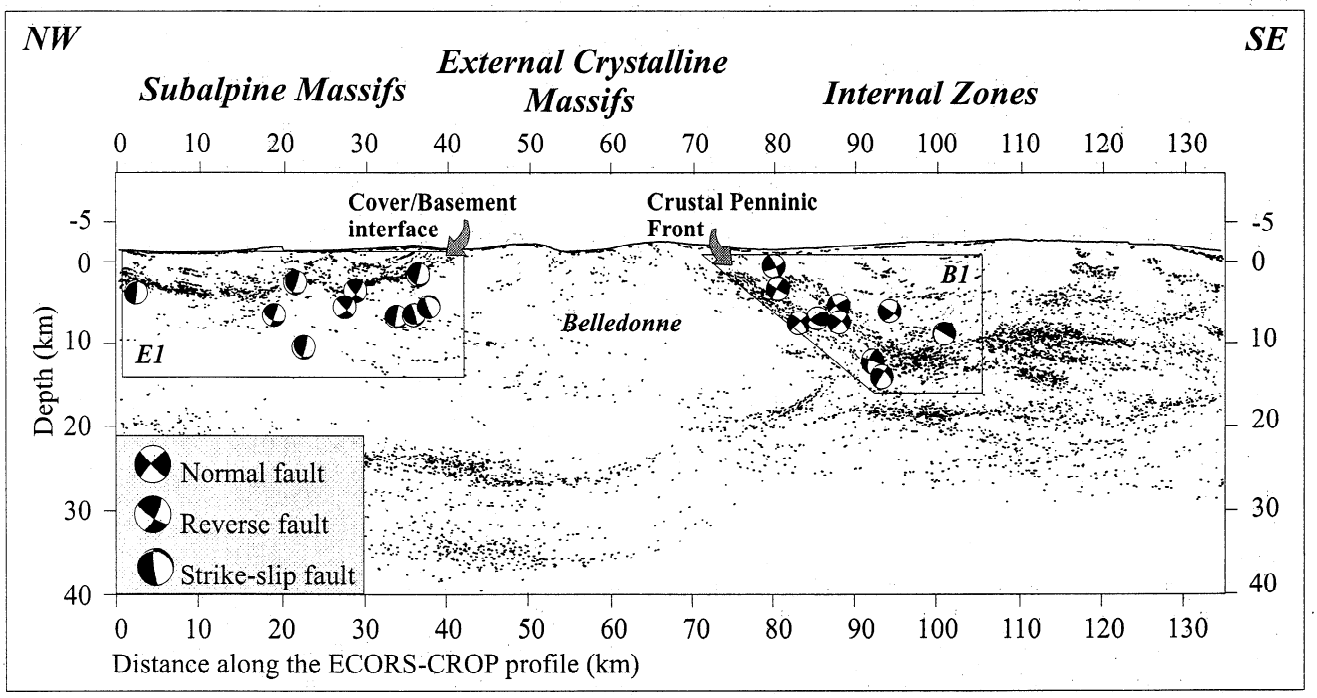

Figure 4. Crustal cross section along dashed line AA' of Figure 2b across the *E1* and *B1* seismotectonic domains and the Belledonne crystalline massif. The ECORS-CROP vertical-reflection-seismic migrated line drawing (20 km to the north) [*Sénéchal and Thouvenot*, 1991] and all the focal mechanisms of the *E1* and *B1* domains are projected onto the cross section. Arrows indicate reflectors associated with the cover/basement interface between the subalpine massifs and the external crystalline basement, and with the boundary between the external and internal zones (CPF, equivalent in this part of the Alps to the Frontal Penninic Thrust of the ECORS-CROP profile). Normal faulting is localized in the hangingwall of the CPF, suggesting it is now inverted as an extensional crustal detachment. Compressive tectonics at the front of the external crystalline massifs involve the crystalline basement.

affected by extension. Figure 6 shows the azimuth of near-horizontal principal stress axes, σ_1 and/or σ_3. Similar inversions were previously performed in other parts of the Alps and results by *Eva et al.* [1997] southeast of Torino (Italy), and *Maurer et al.* [1997] between the Aar and Mont-Blanc massifs (Valais region, Switzerland), are also shown to enable an overall discussion on the stress field of the western Alps.

The first striking feature of this stress map (Figure 6) is that minimum-stress axes (σ_3) computed just east of the CPF trend radially to the Alpine arc, over more than 300 km along the range strike. Generally, the CPF defines the outer (western) limit of the area undergoing extension. However, extension spreads across the CPF in the saddle between the Pelvoux and Argentera basement massifs, i.e., into the *E2* domain. This domain aside, the radial extension localized in the hangingwall of the CPF remains perpendicular to this former thrust. This stress field (Figure 6) and the location of earthquakes close to the CPF (Figure 2b and Figure 4) suggest that it works currently as an extensional crustal detachment. The stress tensor computed for the *P* domain shows that extension is not only localized close to the CPF but extends to the innermost zones of the belt as well. The fairly straight shape of the Piemont seismic arc and the oblique σ_3 direction, which both crosscut the arcuate surface structures, indicate that seismicity in this domain is associated with more deep-seated and straight structures such as the Ivrea body.

Large-scale stress maps [*Müller et al.*, 1992; *Grünthal and Stromeyer*, 1992] document the still-active collision between stable Europe and the Adriatic promontory. These maps show fanning compression trajectories, perpendicular to the leading edge of the indenter. This is confirmed by the stress field at the limits of the Alpine chain inferred from the stress inversion in the *E1* domain and from that performed by *Maurer et al.* [1997] north of the CPF and by *Eva et al.* [1997] east of the Piemont seismic arc. The counterclockwise rotation of the Adriatic indenter is compatible with the strike-slip focal mechanisms in the northwestern external Alps and their associated stress tensor [*Maurer et al.*, 1997]. Although our stress map (Figure 6) agrees with the European stress field at the limits of the belt, the

Table 2. Focal Solutions Parameters for the *E1* Domain

N	D	date	h	mn	sec	lat	lon	depth	mag	phiP	dipP	phiT	dipT
80	E1	923009	1	54	34	45-09	5-52	6	2.3	253	1	343	28
81	E1	940204	22	19	47	45-23	6-04	7	2,0	259	4	168	18
82	E1	940725	0	18	57	45-11	5-53	2	1.8	263	3	171	25
83	E1	941214	8	55	59	45-57	6-25	7	5.1	281	16	173	49
84	E1	950425	13	2	58	45-51	5-58	4	2.1	84	11	354	4
85	E1	950828	12	42	30	45-33	6-07	6	2.3	315	4	205	69
86	E1	950904	17	2	54	45-42	6-12	11	2.9	273	3	181	25
87	E1	950904	21	1	40	45-42	6-11	3	2.8	93	1	183	28
88	E1	950908	16	46	57	45-12	5-54	7	2.5	268	18	359	4
89	E1	951224	4	5	6	45-29	6-04	4	1.8	305	4	205	69

Same captions as Table 1. Data after *Thouvenot* [1996].

Table 3: Stress-Tensor Parameters

Seismic domain	Code	N	σ1		σ2		σ3		R	M
			tr	pl	tr	pl	tr	pl		
*Stereonets**										
Sub-Alpine	*E1*	10	263	5	171	24	5	65	0.5	2.6
Flysh nappe	*E2*	15	156	66	6	21	272	11	0.5	5.2
West Piemont	*P*	14	23	53	117	34	276	12	0.9	4.7
North Briançonnais	*B1*	9	146	73	39	5	308	16	0.6	2.7
Central Briançonnais	*B2*	20	4	73	169	16	260	4	0.5	5.1
South Briançonnais	*B3*	10	173	49	334	39	72	9	0.6	3.9
Eva et al. [1997] and Maurer et al. [1997]†										
East Piemont		14	282	5	180	22	23	67	0.6	4.7
North Valais		8	302	24	186	46	50	35	0.4	1.7
South Valais		10	255	63	100	25	5	10	0.4	2.2
Global inversion‡										
Internal domains	*B1,B2,B3,P*	53	190	67	24	22	262	5	0.6	8.3
Southern domains	*E2,B3,P*	39	28	51	246	33	143	19	0.8	8.9

N, number of focal solutions used in each inversion; tr,pl, trend and plunge of the axis; R, shape ratio of the stress ellipsoid; M, misfit. Inversions were performed using Gephart's method.

*Stress-tensor parameters corresponding to the Stereonets of Figure 5 for Domains *E1*, *E2*, *B1*, *B2*, *B3*, and *P*.

†Stress-tensor parameters found by *Eva et al.* [1997] and *Maurer et al.* [1997] are listed for comparison.

‡Stress-tensor parameters corresponding to the inversion performed with the focal solutions of the internal domains as a whole (*B1*, *B2*, *B3* and *P*) and of the three southern domains (*E2*, *B3*, and *P*).

unexpected widespread extension in the core of the western Alpine arc cannot be explained by simple collision-related tectonics.

4. Discussion and Conclusion

Such a highly inhomogeneous intrabelt stress field, with widespread radial extension in the central part of the western Alpine arc, calls for a new geodynamic model of this active collision belt. It makes clear that current tectonics in this mountain belt are different from earlier Tertiary deformation, which is dominated by collision-related radial crustal shortening. Several geodynamic models have been proposed to explain synorogenic extension, but none is fully satisfactory.

1. Tibetan-like or Basin-and-Range-like tectonics [e.g., *Ménard and Molnar,* 1988; *Molnar and Lyon-Caen,* 1988] imply gravitational collapse and spreading of an overthickened crust to explain extension. These models can therefore explain why extensional tectonics affect high-elevation areas such as the Andes [e.g., *Isacks*, 1988; *Meijer et al.,* 1997], but they are not consistent with the rather low average altitude of the extensional area in the core of the western Alps (~1500 m), and of the Alps in

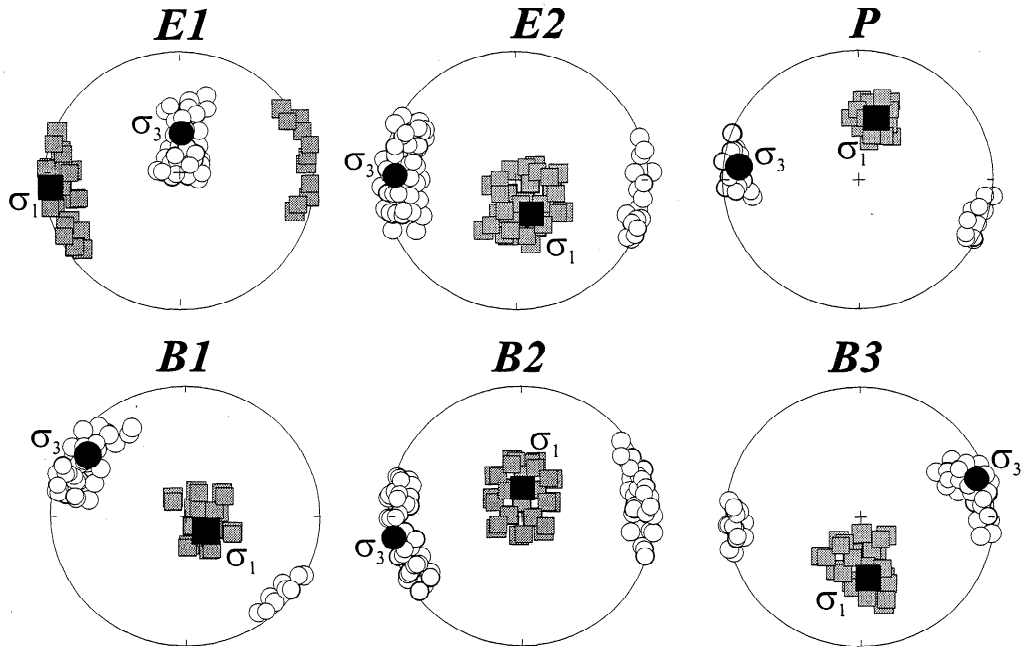

Figure 5. Stress-tensor stereonets inverted for the six seismic domains (lower hemisphere, equal area). Squares are σ_1, circles are σ_3, black is best solution, and grey squares and white circles are 95% confidence domains for σ_1 and σ_3, respectively. Corresponding parameters are listed in Table 3.

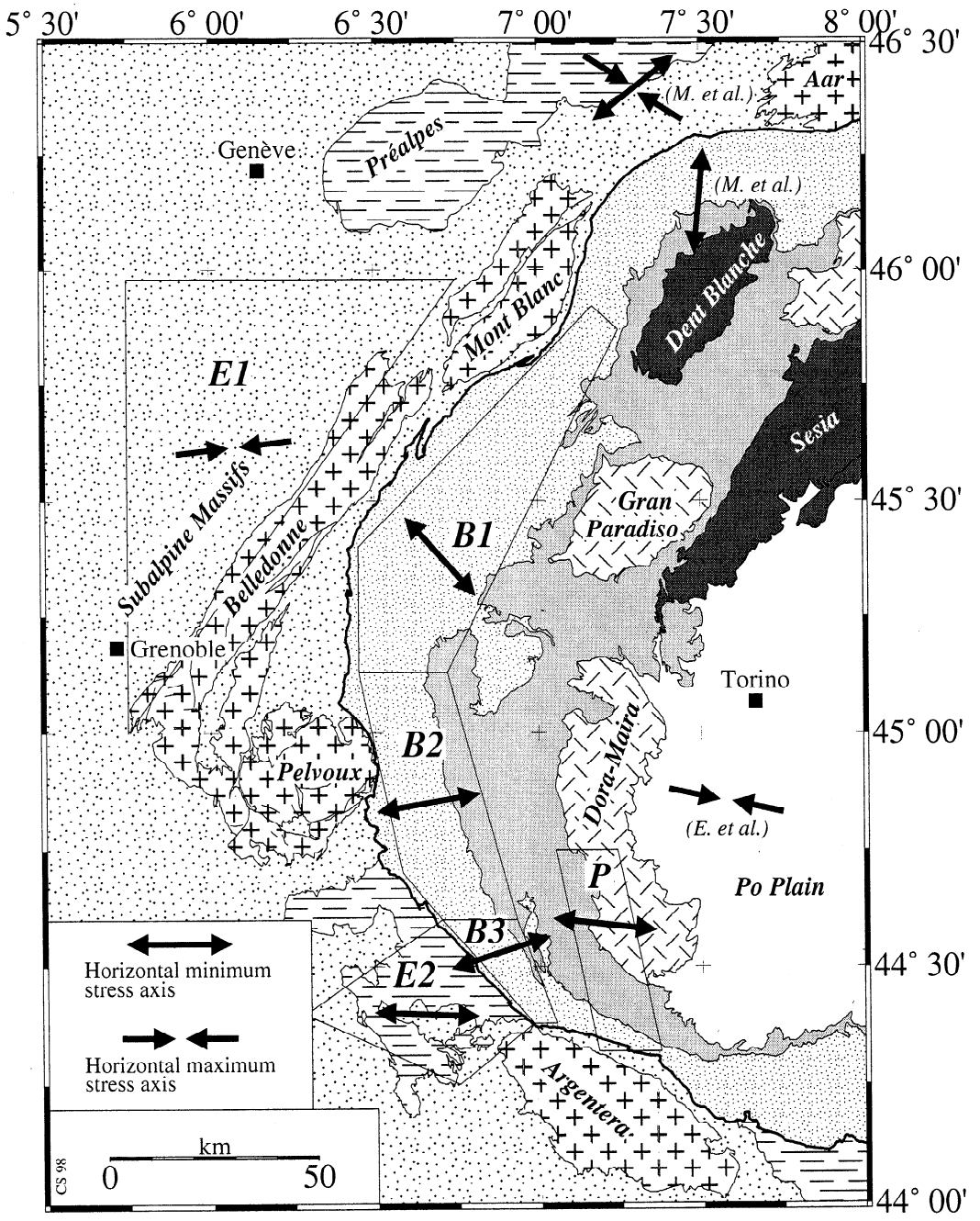

Figure 6. Map of the stress tensors computed in this study, completed by three tensors from *Maurer et al.* [1997] (*M. et al.*) and *Eva et al.* [1997] (*E. et al.*). Same caption as in Figure 1. Principal stress axes are shown as convergent arrows for σ_1 and divergent ones for σ_3. Extension is widespread, radial to the arcuate geometry of the belt, and sandwiched between two compressive domains.

general, where the crust is thick (~50 km) but not as thick as the Tibetan one [*ECORS-CROP Deep Seismic Sounding Group*, 1989]. Mean focal depths for events drawn on Figure 2a along the Briançonnais arc (around 8 km) and along the Piemont arc (around 12 km) also make clear that extension is not restricted to shallow depth but affects the upper 15 km of the crust. The context of this extension in such a low-altitude area is therefore very different from the shallow extension observed in many high-altitude mountain belts elsewhere in the world.

2. General transtensive tectonics associated with the counterclockwise rotation of the Adriatic indenter [*Anderson and Jackson*, 1987; *Ménard*, 1988; *Vialon et al.*, 1989] seem to be quite pertinent to explain at least part of the extension observed to the north of the Alpine arc [*Maurer et al.*, 1997] and in the central Alps, southeast of the Aar massif [*Roth et al.*, 1992]. Nevertheless, this rotation model is not compatible with radial extension as far to the south as the Argentera massif. Moreover, south of Briançon, where the trend of the Alpine arc is NNW-SSE oriented, compression rather than extension would be expected for this model.

3. Another possibility is extension in the extrados of a crustal-scale thrust-ramp anticline [e.g., *Eva et al.*, 1997]. This model

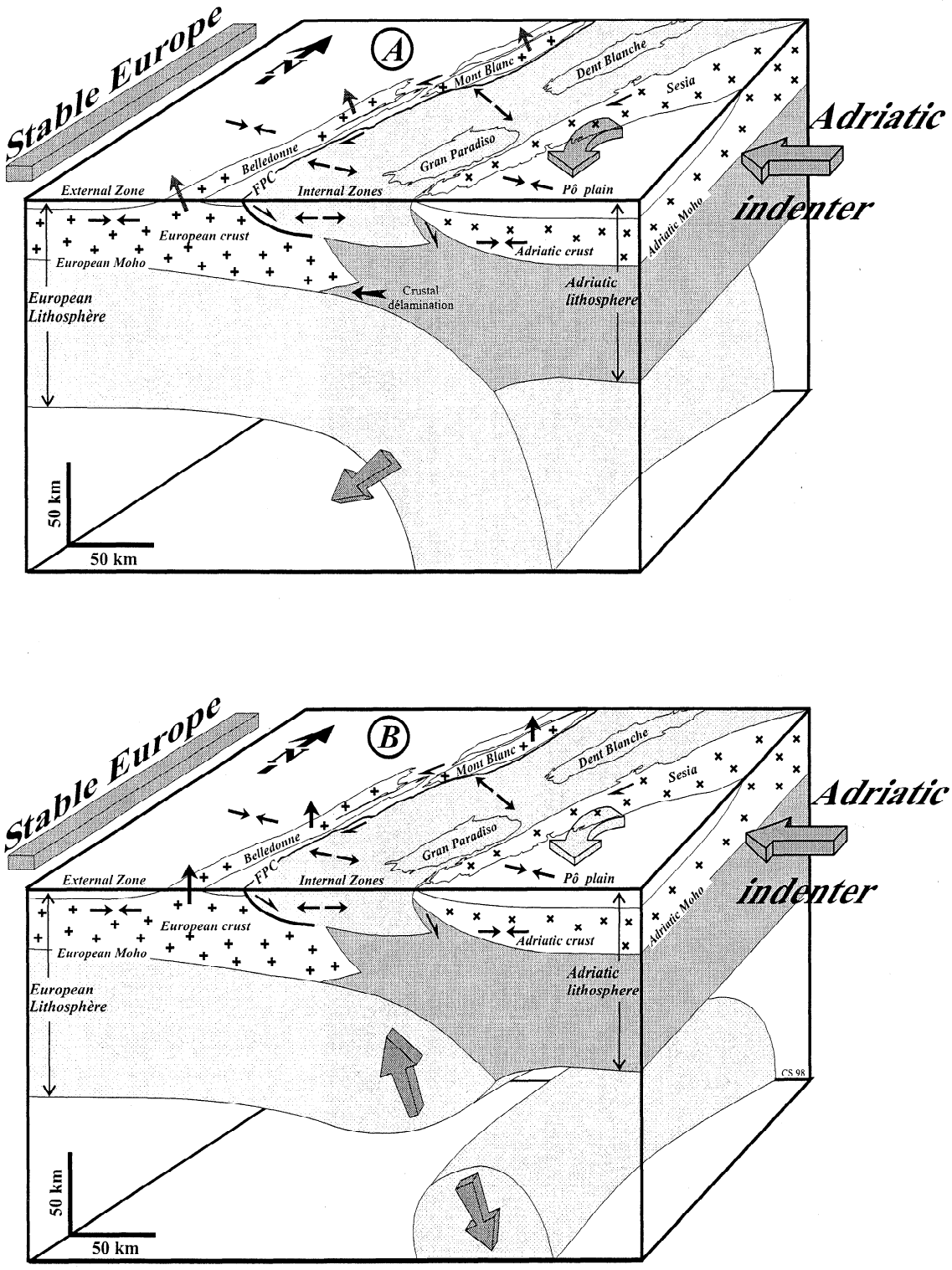

Figure 7. Block diagrams across the western Alpine arc showing the relationships between lithospheric structures and present tectonics. The front of the block diagrams roughly follows a WNW-ESE cross section between Grenoble and Torino. The top faces show the main structural units (CPF, Crustal Penninic Front). Main crustal structures, which can be followed to the north into the Swiss Alps (such as mantle slices and CPF geometry) [*Valaseck and Müller,* 1997], are drawn from the ECORS-CROP seismic profile [*ECORS-CROP Deep Seismic Sounding Group,* 1989]. Adria indentation and its counterclockwise rotation with respect to stable Europe are symbolized by the thick arrow on the right of the block and by the curved arrow beneath the Po Plain, respectively. (a) The subduction of the continental passive margin of the Tethys, facilitated by a crustal delamination may act as a slab retreat and rollback. Extension in the internal Alps is here compared to back arc extension. (b) Slab break-off would drive the uplift of the belt as a whole, especially that of the external crystalline massifs, while extension would affect the adjacent internal zones, with tectonic inversion of major crustal discontinuities.

implies high-altitude internal zones, whereas the belt crest of the western Alps follows the External Crystalline Massifs, and the internal zones exhibit much lower average altitudes. Also, shallow normal-faulting focal mechanisms would be associated with deeper-seated reverse faulting, related to the activity along the crustal thrust ramp, which is not seen in the present study.

4. A fourth model, dominated by compression, implies vertical extrusion. Late Alpine ductile to brittle horizontal extension in the Piemont Zone [*Schwartz et al.*, 1999] is thought to develop above an ascending mantle indenter. This kind of model can account for present-day extension along the Piemont seismic arc, but it fails to explain the widespread extension to the west, along the Crustal Penninic Front.

Consequently, none of the models presented above is able to explain the widespread extension in the core of the western Alpine arc as a whole. We alternatively propose that buoyancy forces actually drive this extension, which seems to fit better several characteristics of the western Alps. Figure 7 illustrates two variants of such a mechanism; in both cases, intrabelt lithospheric buoyancy forces responsible for the extensional tectonics in the core of the belt are superimposed onto the general effects of the ongoing collision (indentation and rotation of the Adriatic indenter with respect to stable Europe). Such contrasted tectonics imply lithospheric instability driven by the subducted European slab beneath the belt, first proposed by *Panza and Müller* [1979]. In the western Alps, several studies using ray-tracing techniques suggest such a slab-like structure [*Spackman*, 1990; *Guyoton*, 1991; *Kissling*, 1993], whereas teleseismic tomography only shows a velocity contrast (low velocity beneath Europe, high velocity beneath Adria) [*Cattaneo and Eva*, 1990; *Thouvenot*, 1996].

In a subduction-retreat and slab-rollback model, extension in the internal zones of the Alps can be compared to back-arc spreading (Figure 7a). Nevertheless, the geodynamic context is here an advanced continental collision with the subduction of the northern continental passive margin of the Tethys ocean, facilitated by a crustal delamination. Such a model may explain the tectonic contrast between the transpressive regime to the front of the belt and the extension in the core of the belt.

The extensional tectonics evidenced by this study can also be explained by detachment of the subducted European lithosphere (Figure 7b), a phenomenon already proposed for the northwestern Alps by *Lyon-Caen and Molnar* [1989] to explain the uplift of the Alps as a whole (especially the external crystalline massifs) and of the Molasse basin. Such vertical motions have been documented in the central Alps [*Schaer and Jeanrichard*, 1974] and across the Belledonne massif [*Fourniguet*, 1977], even if they remain poorly constrained in the western Alps. *Seward and Mancktelow* [1994] also provide evidence for a recent uplift of the external crystalline massifs using fission-track analysis. This kind of model has been proposed for the eastern and central Alps for the Oligocene [*Blanckenburg and Davies*, 1995]. For the western Alps, thermal anomaly (including magmatism) associated to a slab break-off is not observed. Nevertheless, a young (e.g. Pliocene) break-off [*Lyon-Caen and Molnar*, 1989] may have occurred with a delay in the heat flow propagation. The slab break-off would have unbalanced the belt, resulting in uplift of the external zone and extension in the internal zones. In this model, the CPF and the western flank of the Ivrea body both act as inherited weakness zones, the tectonic inversion along these crustal discontinuities concentrating the extensional deformation.

These two models take into account the extension of the core of the western Alps (a low-altitude area), the uplift of the external crystalline massifs, and the reactivation of inherited crustal structures. Nevertheless, it remains poorly constrained and new geophysical investigations such as GPS measurements or heat flow measurements are needed to better understand the present-day dynamics of the region. Compression in the Po plain and to the front of the belt, i.e., at the limits of the belt, is probably linked to ongoing collision processes interfering with the slab behavior (rollback or break-off). Thus the complex current tectonics of the western Alps would result from the interference of the following driving mechanisms: Europe-Adria collision and relative rotation at the limits of the belt, and buoyancy forces within the western Alpine lithosphere.

Acknowledgments. IGG (Genova, Italy) kindly exchanged seismological data on the Italian side of the Alps. Maps were prepared using GMT software [*Wessel and Smith*, 1991]. We thank J.W. Gephart for making available his program code. We are also very grateful to M. Burkhard for providing the Swiss stress-tensor parameters and to P. Van der Beek for his helpful comments on the manuscript. We also thank R. M. Russo, S. Schmid, and an anonymous reviewer for providing highly constructive reviews.

References

Amelung, F., and G. King, Large-scale tectonic deformation inferred from small earthquakes, *Nature*, *386*, 702-705, 1997.

Anderson, H., and J. Jackson, Active tectonics in the Adriatic region, *Geophys. J. R. Astron. Soc.*, *91*, 937-983, 1987.

von Blanckenburg, F., and J.H. Davies, Slab breakoff: A model for syncollisional magmatism and tectonics in the Alps, *Tectonics*, *14(1)*, 120-131, 1995.

Cattaneo, M., and C. Eva, Propagation anomalies in northwestern Italy by inversion of teleseismic residuals, *Terra Nova*, 2, 577-584, 1990.

Coward, M.P., D. Dietrich, and R.G. Park (Eds.), Alpine tectonics, *Geol. Soc. Spec. Publ.*, *45*, 1989.

DeMets, C., R.G. Gordon, D.F. Argus, and S. Stein, Current plate motions, *Geophys. J. Int.*, *101*, 425-478, 1990.

ECORS-CROP Deep Seismic Sounding Group, A new picture of the Moho under the western Alps, *Nature*, *337*, 249-251, 1989.

Eva, E., S. Solarino, C. Eva, and G. Neri, Stress tensor orientation derived from fault plane solution in the southwestern Alps, *J. Geophys. Res.*, *102*, 8171-8185, 1997.

Eva, E., S. Pastore, and N. Deichmann, Evidence for ongoing extensional deformation in the western Swiss Alps and thrust-faulting in the southwestern Alpine foreland, *J. Geodyn.*, *1*, 27-43, 1998.

Fourniguet, J., Mise en évidence de mouvements néotectoniques actuels verticaux dans le Sud-Est de la France par comparaison de nivellements successifs, *Rap. BRGM 77SGN081GEO*, pp. 1-35, Bur. des Rech. Geol. et Min., Orléans, France, 1977.

Fréchet J., Sismicité du sud-est de la France et une nouvelle méthode de zonage sismique, Thesis, Univ. Sci. Technol. Medic., Grenoble, France, 1978.

Fréchet, J., and N. Pavoni, Etude de la sismicité de la zone briançonnaise entre Pelvoux et Argentera (Alpes occidentales) à l'aide d'un réseau de stations portables, *Eclogae Geol. Helv.*, *72*(3), 763-779, 1979.

Gephart, J.W., Fmsi : A Fortran program for inverting fault/slickenside and earthquake focal mechanism data to obtain the regional stress tensor, *Comput. Geosci.*, *16*(7), 953-989, 1990.

Gephart, J. W., and W.D. Forsyth, An improved method for determining the regional stress tensor using earthquake focal mechanism data: Application to the San-Fernando earthquake sequence, *J. Geophys. Res.*, *89*, 9305-9320, 1984.

Grünthal, G., and D. Stromeyer, The recent stress field in central Europe: Trajectories and finite element modeling, *J. Geophys. Res.*, *97*, 11,805-11,820, 1992.

Guyoton, F., Sismicité et structure lithosphérique des Alpes occidentales, Thesis, Univ. J. Fourier, Grenoble, France, 1991.

Isacks, B.L., Uplift of the central Andean plateau and bending of the Bolivian orocline, *J. Geophys. Res.*, *93*, 3211-3231, 1988.

Kissling, E., Deep structure of the Alps – What do we really know ?, *Phys. Earth Planet. Inter., 79*, 87-112, 1993.

Lee, W.H., and J.E. Lahr, HYPO71: A computer program for determining hypocenter, magnitude and first-motion pattern of local earthquakes, *U.S. Geol. Surv. OpenFile Rep. 75-331*, 1975.

Lyon-Caen, H., and P. Molnar, Constraints on the deep structure and dynamic processes beneath the Alps and adjacent regions from analysis of gravity anomalies, *Geophys. J. Int., 99*, 19-32, 1989.

Maurer, H., M. Burkhard, N. Deichmann, and G. Green, Active tectonism in the central Alps: Contrasting stress regimes north and south of the Rhone Valley, *Terra Nova, 9*, 91-94, 1997.

Meijer, P.T., R. Govers and M.J. Wortel, Forces controlling the present-day state of stress in the Andes, *Earth Planet. Sci. Lett., 148*, 157-170, 1997.

Ménard, G., Structure et cinématique d'une chaîne de collision: Les Alpes occidentales et centrales, thesis, Univ. J. Fourier, Grenoble, France, 1988.

Ménard, G., and P. Molnar, Collapse of a Hercynian Tibetan Plateau into a late Palaeozoic European Basin and Range province, *Nature, 334*, 235-237, 1988.

Ménard, G., and F. Thouvenot, Ecaillage de la lithosphère européenne sous les Alpes occidentales: arguments gravimétriques et sismiques liés à l'anomalie d'Ivrea, *Bull. Soc. Geol. Fr., 26*, 875-884, 1984.

Molnar, P., and H. Lyon-Caen, Some simple physical aspects of the support, structure, and evolution of mountain belts, *Spec. Pap. Geol. Soc. Am., 218*, 179-207, 1988.

Müller, B., M.L. Zoback, K. Fuchs, S. Gregersen, N. Pavoni, O. Stephansson, and C. Ljunggren, Regional patterns of tectonic stress in Europe, *J. Geophys. Res., 97*, 11783-11803, 1992.

Nicolas, A., A. Hirn, R. Nicolich, R. Polino, and ECORS-CROP Working Group, Lithospheric wedging in the western Alps inferred from the ECORS-CROP traverse, *Geology, 18*, 587-590, 1990.

Panza, G.F., and S. Müller, The plate boundary between Eurasia and Africa in the Alpine area, *Mem. Sci. Geol. Padova, 33*, 43-50, 1979.

Paul, A., F. Thouvenot, J. Fréchet, M. Cattaneo, D. Spallarossa, and N. Bethoux, Local earthquake tomography of the south-western Alps (Géofrance 3D 1996 experiment), *Abstract Suppl. 1, 16 EGS*, Eur. Geophys. Soc., London, 1998.

Pavoni, N., Crustal stresses inferred from fault plane solutions of earthquakes and neotectonic deformations in Switzerland, *Rock Mech., Suppl. 9*, 63-68, 1980.

Pavoni, N., and P. Roth, Seismicity and seismotectonics of the Swiss Alps: Results of microearthquake investigations 1983-1988, in *Deep Structures of the Alps*, edited by F. Roure, P. Heitzmann, and R. Polino, *Mem. Hors Ser. Soc. Geol. Fr., 156*, 129-134, 1990.

Reasenberg, P.A., and D.H. Oppenheimer, FPFIT, FPPLOT and FPPAGE: Fortran computers programs for calculating and displaying earthquake fault-plane solutions, *US. Geol. Surv. Open File Rep. 85-739*, 1985.

Rey, D., T. Quarta, P. Mouge, M. Miletto, R. Lanza, A. Galdeano, M.T. Carrozzo, R. Bayer, and E. Armando, Gravity and acromagnetic maps of the western Alps: Contribution to the knowledge of the deep structures along the ECORS-CROP seismic profile, in *Deep Structures of the Alps*, edited by F. Roure, P. Heitzmann, and R. Polino, *Mem. Hors Ser. Soc. Géol. Fr., 156*, 107-121, 1990.

Roth, P., N. Pavoni, and N. Deichmann, Seismotectonics of the eastern Swiss Alps and evidence for precipitation-induced variations of seismic activity, *Tectonophysics, 207*, 83-97, 1992.

Rothé, J.P., Les séismes des Alpes françaises en 1938 et la sismicité des Alpes occidentales, *Ann. Inst. Phys. Globe Strasbourg, 3*, 1-105, 1941.

Schaer, J.P., and F. Jeanrichard, Mouvements verticaux anciens et actuels dans les Alpes suisses, *Eclogae Geol. Helv., 67*, 101-119, 1974.

Schwartz, S., J.M. Lardeau, A. Paul, M. Cattaneo, P. Tricart, S. Guillot, Y. Laggabrielle, and G. Poupeau, Syn-convergence extension, mantle indentation and exhumation of high-pressure rocks: insights from the western Alps, *Abstract Suppl. EUG 10*, Eur. Union. Geosci., Strasbourg, 1999.

Sellami, S., E. Kissling, F. Thouvenot, and J. Fréchet, Initial reference velocity model for seismic tomography in the western Alps, *Abstract Suppl. EGS 20*, Eur. Geophys. Soc. London, 1995.

Sénéchal, G., and F. Thouvenot, Geometrical migration of line-drawing: A simplified method applied to ECORS data, in *Continental Lithosphere: Deep Seismic Reflections, Geodyn. Ser.*, vol. 22, edited by R. Meissner et al., pp. 401-407, AGU, Washington D.C., 1991.

Seward, D., and N. Mancktelow, Neogene kinematics of the central and western Alps: Evidence from fission-track dating, *Geology, 22*, 803-806, 1994.

Spackman, W., Tomographic images of the upper mantle below central Europe and the Mediterranean, *Terra Nova, 2*, 542-553, 1990.

Solarino, S., E. Kissling, S. Sellami, G. Smriglio, F. Thouvenot, M. Granet, K. Bonjer, and D. Slejiko, Compilation of a recent seismicity data base of the greater Alpine region from several seismological networks and preliminary 3D tomographic results, *Ann. Geofis., 11*, 161-174, 1997.

Sue, C., Dynamique actuelle et récente des Alpes occidentales internes – Approche structurale et sismologique, Thesis, Univ. J. Fourier, Grenoble, France, 1998.

Sue, C., and P. Tricart, Late Alpine brittle extension above the Frontal Penninic Thrust near Briançon, western Alps, in press, *Eclogae Geol. Helv.*, 1999.

Tapponnier, P., Evolution tectonique du système alpin en Méditerranée : Poinçonnement et écrasement rigide-plastique, *Bull. Soc. Geol. Fr., 7*, 437-460, 1977.

Thouvenot, F., Aspects géophysiques et structuraux des Alpes occidentales et de trois autres orogènes: Atlas, Pyrénées, Oural, Thesis, Univ. J. Fourier, Grenoble, France, 1996.

Thouvenot, F., J. Fréchet, F. Guyoton, R. Guiguet, and L. Jenatton, SISMALP: An automatic phone-interrogated seismic network for the western Alps, *Cah. Cent. Eur. Geodyn. Seismol., 1*, 1-10, 1990.

Tricart, P., From passive margin to continental collision: A tectonic scenario for the western Alps, *Am. J. Sci., 284*, 97-120, 1984.

Valaseck, P., and S. Müller, 3D tectonic model of the central Alps based on an integrated interpretation of seismic refraction and NRP20 reflection data, in *Results of NRP20: Deep structure of the Swiss Alps*, edited by O.A. Pfiffner et al., pp 305-325, Birkhäuser Verlag, Basel, 1997.

Vialon, P., P. Rochette, and G. Ménard, Indentation and rotation in the western Alpine arc, in *Alpine Tectonics*, edited by M.P. Coward, D. Dietrich, and R.G. Park, *Geol. Soc. Spec. Publ., 45*, 329-338, 1989.

Wessel, P., and W.H.F. Smith, Free software helps map and display data, *Eos Trans. AGU, 72*, 441 and 445-446, 1991.

J. Fréchet and F. Thouvenot, Laboratoire de Géophysique Interne et Tectonophysique, Observatoire de Grenoble, BP53, F-38041 Grenoble cedex 9, France. (Francois.Thouvenot@obs.ujf-grenoble.fr; Julien.Frechet@obs.ujf-grenoble.fr)

C. Sue, Institut de Géologie, Université de Neuchâtel, rue Argand, 11, CH-2007 Neuchâtel, Switzerland. (christian.sue@geol.unine.ch)

P. Tricart, Laboratoire de Géodynamique des Chaînes Alpines, 15 rue M. Gignoux, F-38000 Grenoble, France. (Pierre.Tricart@ujf-grenoble.fr)

(Received October 8, 1998; revised May 18, 1999; accepted July 13, 1999.)